**Supplementary Information**

# Pressure-induced phase transition on layered $HgPSe_3$ revealed by optical, structural and vibrational studies

Beatriz de Simoni,[‡*a] Robert Oliva,[‡b] Miłosz Rybak,[a] Jan Kopaczek,[a] Agata K. Tołłoczko,[a] Jordi Ibañez,[b] Filip Dybała,[a] Paweł Scharoch,[a] Iva Plutnarová,[c] Zdeněk Sofer,[c] Óscar Gomis,[d] Pablo Botella,[e] Daniel Errandonea,[e] Nikolas Antonatos,[**a] Robert Kudrawiec [a]

[a]Department of Semiconductor Materials Engineering, Wroclaw University of Science and Technology, Wybrzeże Wyspiańskiego 27, 50-370 Wrocław, Poland
[b]Geosciences Barcelona (geo3bcn-CSIC), C/ Lluís Solé i Sabarís s/n, 08028 Barcelona, Catalonia, Spain
[c]Department of Inorganic Chemistry, University of Chemistry and Technology Prague, Technická 5,166 28 Prague 6, Czech Republic
[d]Centro de Tecnologías Físicas, MALTA Consolider Team, Universitat Politècnica de València, 46022 València, Spain
[e]Department of Applied Physics ICMUV, MALTA Consolider Team, Universitat de València, 46100 Valencia, Spain

Corresponding authors:

* beatriz.desimoni@pwr.edu.pl
** nikolaos.antonatos@pwr.edu.pl

# 1 Decompression data

In order to verify reversibility, decompression data were collected during all experimental techniques and selected data are shown below.

## 1.1 Optical Absorption

Figs. S1 reveal that the lineshape of the absorption edge is almost identical upon pressure release, with a more quadratic dependence (and steeper slope) in the low-pressure regime compared to the high-pressure phase (with a clear square-root lineshape), indicating a transition back from an indirect to a quasi-direct bandgap. Furthermore, the original color of the sample is also recovered upon decompression, as confirmed by the optical images.

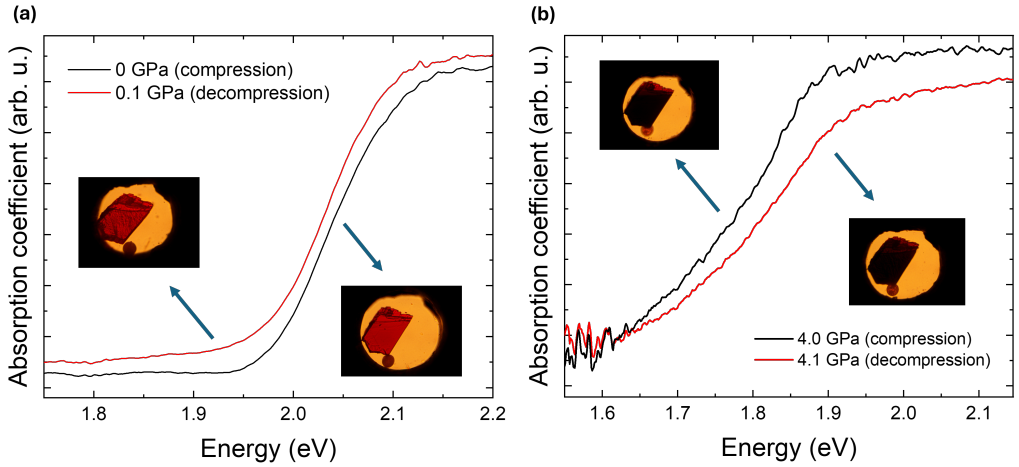


**Fig. S1:** Absorption coefficient and optical images during compression and decompression at approximately (a) 0 GPa and (b) 4 GPa.

## 1.2 Raman Spectroscopy

In general, the peak positions are recovered after pressure release. The differences in peak positions observed in Figs. S2 are due to slight differences in pressure values. While the main Raman modes are restored upon decompression, some minor features observed during compression are no longer detected.

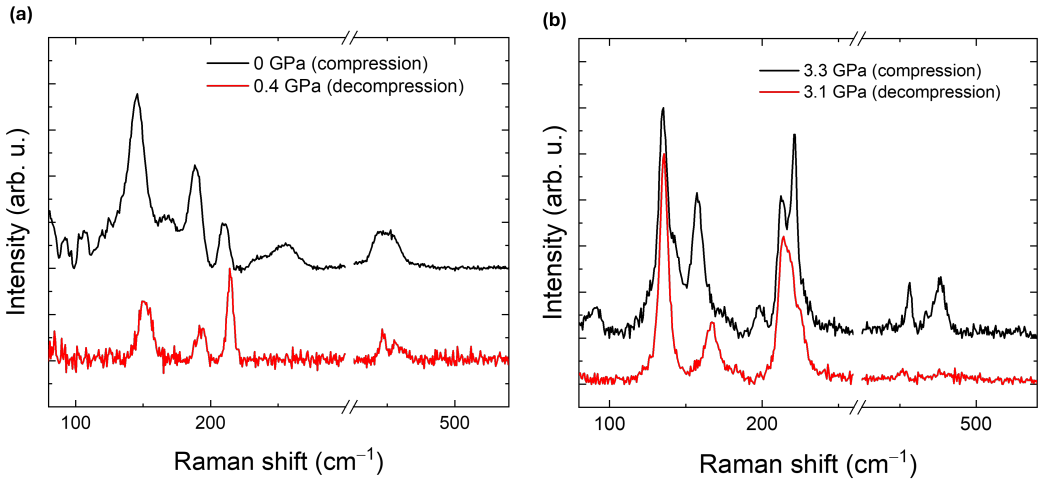


**Fig. S2:** Raman spectra recorded during compression and decompression at approximately (a) 0 GPa and (b) 3 GPa. The main spectral features are present in all measurements.

## 1.3 X-ray diffraction

Figs. S3 compare the diffraction patterns acquired at approximately 3 and 6 GPa during compression and decompression. Upon decompression, most diffraction peaks disappear, while the remaining ones become significantly weaker and broader, suggesting possible partial amorphization of the sample. Despite this, we still observe strong evidence of a structural transition back to the original structure between 6 and 3 GPa. This can only be evidenced from the lowest angle peaks since these are unambiguously assigned. While peaks below 7.5° remain unchanged, a characteristic splitting and a doubling of diffraction peaks take place in the 7.5-9° range, as shown in Fig. S4. As it can be seen in the left panel of the figure, upon compression the peak at 7.7° (which corresponds to the (004) and (-131) reflections) splits into two main peaks at 6.1 GPa, with the splitting starting at 3.8 GPa, which is the transition pressure. The same exact behavior is observed in the downstroke (right panel) where two peaks merge into one from 5.6 GPa down to 2 GPa at 7.5°. On the other hand, an opposite behavior takes place for peaks around 8.5° (corresponding to the (-114) reflection). These peaks merge and become strong above the transition pressure, at 5.0-6.1 GPa. During decompression, the exact same behavior is observed, a strong peak around 8.5° decreases its intensity and results in two peaks as pressure is released, down to 2 GPa.

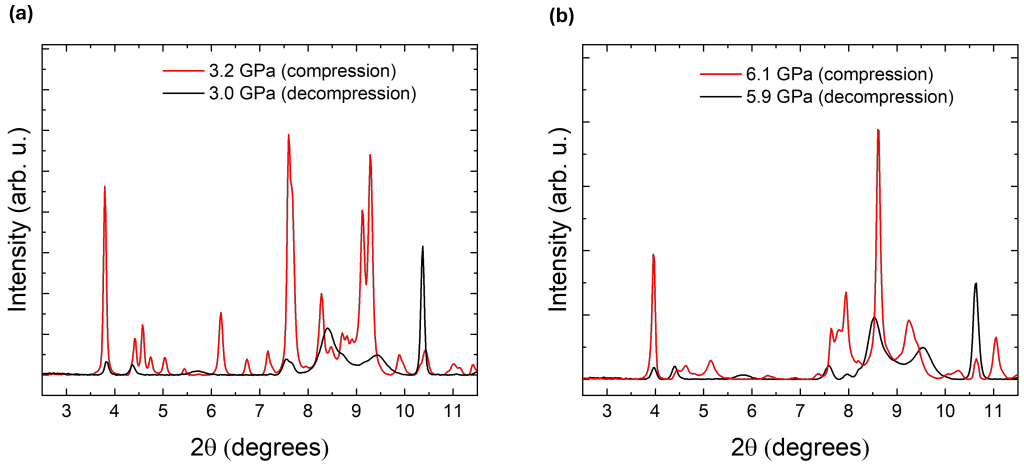


**Fig. S3:** XRD patterns recorded during compression (red) and decompression (black) at approximately (a) 3 and (b) 6 GPa.

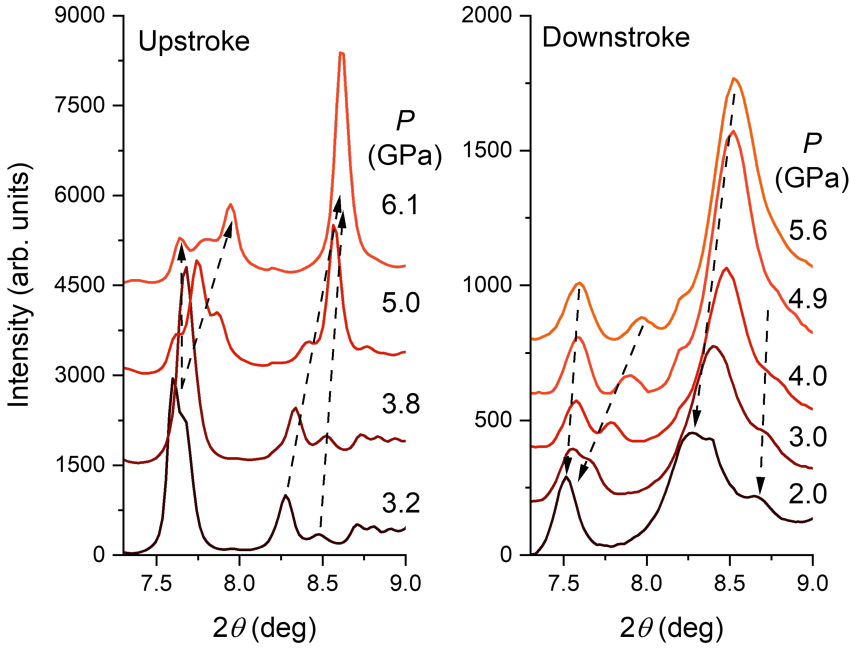


**Fig. S4:** Expanded view of the $2\theta$ range 7.3–9°, highlighting the evolution of the peaks in selected XRD patterns collected during upstroke (left) and downstroke (right).

## 2 Pressure-dependent photoluminescence

Photoluminescence spectroscopy with pressure dependence was performed on $HgPSe_3$ at room temperature for further investigation of the quasi-direct to indirect band gap transition. At 0 GPa, the emission from the sample, centered at around 1.99 eV,[1] overlaps with Raman peaks from the pressure transmitting medium (Daphne 7474) and the diamonds from the diamond anvil cell.[2;3] The emission from the ruby can also be seen, as well as a first-order Raman peak from the diamond, but well separated from the main spectral feature. As pressure increases, the emission from the sample shifts towards lower energies, and at 2.1 and 3.2 GPa it can be clearly seen. At 4.1 GPa, however, the signal from the sample vanishes, since the bandgap becomes indirect as indicated by our optical absorption measurements.

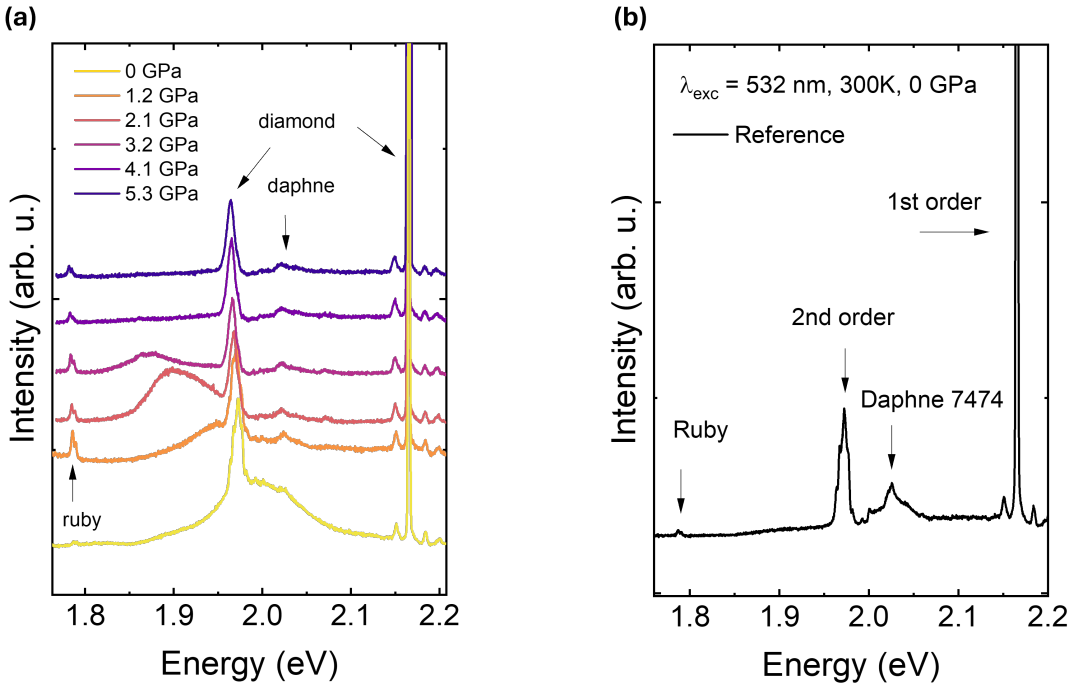


**Fig. S5:** a) Photoluminescence of $HgPSe_3$ with pressure dependence at 300 K, acquired with excitation wavelength 532 nm and laser power of 100 $\mu$W. At 0 GPa, the emission from the sample is overlapped with Raman peaks from the pressure transmitting medium and diamond, as indicated in the reference spectrum in b), which was collected by focusing the laser outside the sample, within the pressure transmitting medium inside the diamond anvil cell.

# 3 X-ray diffraction

Table S1 contains the peak number, experimental, and calculated positions, along with the corresponding Miller indices of the first 16 peaks of the diffraction pattern of $HgPSe_3$ at 0.5 GPa. Such peaks reproduce the expected lattice parameters previously reported under ambient conditions. [4]

**Table S1:** Peak number, observed and calculated peak positions, and hkl assignments of the 16 first peaks from the 0.5 GPa pattern. Calculated peak positions and hkl indices were obtained using DICVOL [5] and FullProf packages [6]

| **Peak label** | $2\theta_{\mathbf{obs}}(^\circ)$ | $2\theta_{\mathbf{calc}}(^\circ)$ | **h** | **k** | **l** |
|---|---|---|---|---|---|
| P1 | 3.64 | 3.615 | 0 | 0 | 2 |
| P2 | 4.35 | 4.325 | 1 | 1 | 0 |
| P3 | 4.50 | 4.4969 | -1 | 1 | 1 |
| P4 | 4.66 | 4.644 | 0 | 2 | 1 |
| P5 | 4.93 | 4.897 | 1 | 1 | 1 |
| P6 | 5.31 | 5.270 | -1 | 1 | 2 |
| P7 | 5.64 | 5.602 | 0 | 2 | 2 |
| P8 | 6.03 | 5.983 | 1 | 1 | 2 |
| P9 | 6.54 | 6.491 | -1 | 1 | 3 |
| P10 | 6.96 | 6.910 | 0 | 2 | 3 |
| P11 | 7.30 | 7.234 | 0 | 0 | 4 |
| P12 | 7.56 | 7.525 | -1 | 3 | 1 |
| P13 | 8.01 | 7.940 | -1 | 1 | 4 |
| P14 | 8.60 | 8.561 | 0 | 4 | 0 |
| P15 | 8.66 | 8.613 | -2 | 2 | 1 |
| P16 | 8.94 | 8.878 | -1 | 3 | 3 |

## 3.1 Le Bail fit at high pressure

Le Bail refinements were performed in order to extract the unit cell parameters at each pressure value. One example is shown in Fig. S6. The fittings were done using FullProf package. [6]

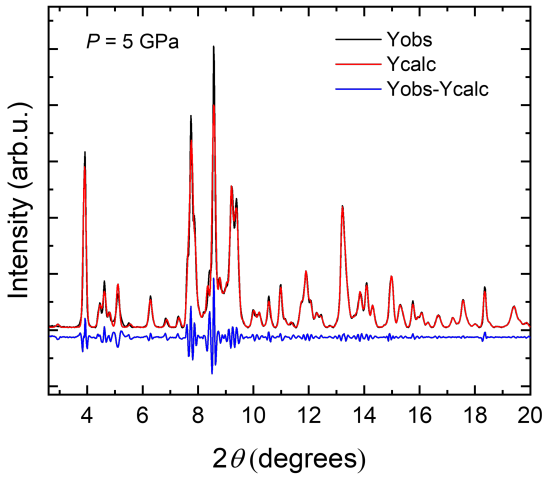


**Fig. S6:** Le Bail fit of the powder diffraction pattern at 5 GPa: observed (red line), calculated (black line), and difference (blue line) profiles are shown.

### 3.2 Axial compressibility - Least-square method

In addition to the Le Bail method, the evolution of the lattice parameters $a, b, c, \alpha, \beta, \gamma$ with increasing pressure was obtained via the least-square method for both monoclinic and high-pressure phases observed above 3.8 GPa from well-identified persisting crystallographic planes (these are $hkl$ = 002, 110, $\bar{1}$10, 021, 111, 112, 023 and 043). It consists of refining the unit-cell parameters through an iterative procedure that minimizes the sum $S$

$$S = \sum_i (d_i^{exp} - d_i^{calc}(a, b, c, \alpha, \beta, \gamma))^2, \tag{1}$$

of squared residuals between measured and calculated interplanar spacing for all peaks $i$ at a given pressure value.[7] Across all peaks from a given pressure value, the least square refinement will find a single set of lattice parameters that minimizes $S$. From Bragg's law equation

$$n\lambda = 2d\sin(\theta), \tag{2}$$

the experimental peak position $2\Theta$ can be converted into interplanar spacing $d$ by

$$d_i^{exp} = \frac{\lambda}{2\sin\theta_i}. \tag{3}$$

The parameter $d_i^{calc}$ is given by the metric-tensor formula

$$\frac{1}{d_{hkl}^2} = H^\top G^{-1} H, \tag{4}$$

where $H = (h, k, l)^\top$ and $G^{-1}$ is the reciprocal-space metric tensor $G$, given by

$$G = \begin{pmatrix} a^2 & ab\cos\gamma & ac\cos\beta \\ ab\cos\gamma & b^2 & bc\cos\alpha \\ ac\cos\beta & bc\cos\alpha & c^2 \end{pmatrix},$$

in its most general form. After the matrix product is done, one gets

$$\begin{aligned} \frac{1}{d_{hkl}^2} = \frac{1}{V^2}[h^2b^2c^2\sin^2\alpha + k^2a^2c^2\sin^2\beta + l^2a^2b^2\sin^2\gamma + l^2a^2b^2\sin^2\gamma + \\ +2hkac^2b(\cos\alpha\cos\beta - \cos\gamma) + 2kla^2bc(\cos\beta\cos\gamma - \cos\alpha) + 2hlab^2c(\cos\gamma\cos\alpha - \cos\beta)], \end{aligned} \tag{5}$$

where the unit cell volume is

$$V = abc\sqrt{1 + 2\cos\alpha\cos\beta\cos\gamma - \cos^2\alpha - \cos^2\beta - \cos^2\gamma}. \tag{6}$$

# 4 Raman Spectroscopy

## 4.1 Polarization-resolved Raman spectroscopy

Backscattering polarization-resolved Raman spectroscopy was performed and the results are shown in Fig. S7. It is observed parallel polarization enhances the intensity of $A_g$ peaks, whereas cross polarization only allows signal from the least intense $B_g$ modes, virtually sharing the same wavenumbers.

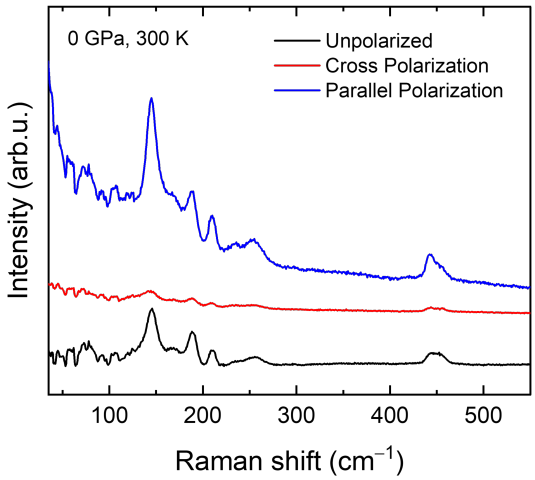


**Fig. S7:** Raman spectra with polarization at ambient conditions reveals that the intensity of all peaks is enhanced under parallel polarization. Spectra are offset vertically for clarity.

The intensity $I$ of a phonon mode is proportional to

$$I \propto |e_s^T \cdot R \cdot e_i|^2, \tag{7}$$

where $e_s$ and $e_i$ are the unit vectors of electric polarization of the scattered and incident light, and $R$ is the Raman tensor. In the case of parallel polarization, $e_s$ and $e_i$ are equal, such as $e_s = e_i = (1, 0, 0)^T$ for pure XX geometry, or $e_s = e_i = (0, 1, 0)^T$ for pure YY geometry. It means that only diagonal terms of $R$ will survive the matrix product and therefore contribute to the intensity. Thus, the peaks observed in Raman spectra correspond to vibrational modes which have nonzero diagonal terms, given by

$$R(A_g) = \begin{bmatrix} a & 0 & d \\ 0 & b & 0 \\ d & 0 & c \end{bmatrix}, \qquad R(B_g) = \begin{bmatrix} 0 & e & 0 \\ e & 0 & f \\ 0 & f & 0 \end{bmatrix},$$

in the case of $C_{2h}$ point group.[8]

## 4.2 Evolution of peaks

Figs. S8 – S10 show detailed plots of the evolution of the peaks in Raman spectra. Peak 1 shifts to lower wavenumbers until 1.5 GPa, while the other peaks shift to higher wavenumbers with different rates, as indicated by their pressure coefficients. Peak positions were obtained by fitting the spectra with Lorentzian functions, and the fits at 0 GPa are shown in blue.

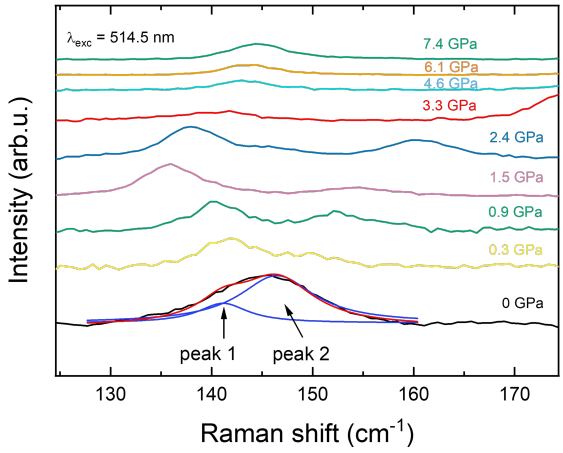


**Fig. S8:** Pressure-dependent evolution of peaks 1 and 2. Lorentzian fits at 0 GPa are shown in blue.

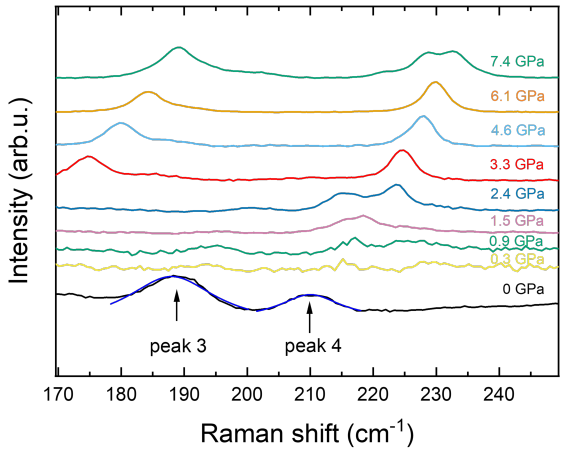


**Fig. S9:** Pressure-dependent evolution of peaks 3 and 4. Lorentzian fits at 0 GPa are shown in blue.

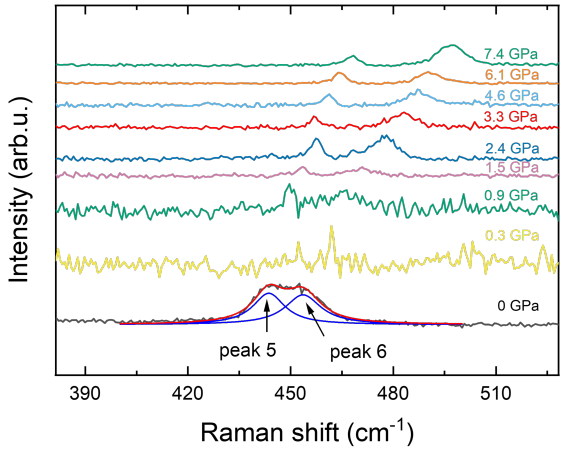


**Fig. S10:** Pressure-dependent evolution of peaks 5 and 6. Lorentzian fits at 0 GPa are shown in blue.

## 4.3 Sample degradation over laser power density and acquisition time

It is well known that $HgPSe_3$ samples (bulk and few-layer) undergo optical degradation under green laser excitation.[9] In order to investigate this, macro-Raman measurements (spot size around 20x250 $\mu$m) at ambient conditions with different acquisition times were performed, and the results are shown in Figs. S11. As can be seen in the figure, an exposure of less than 2.5 mW over an area of 250 $\mu$m spot results in a decrease of Raman signal over time (lower signal-to-noise ratio can be seen for the upper spectra of Fig. S11a. The time-dependency of the integrated overall Raman signal over time is shown in Fig. S11b. A 33% decrease of the Raman signal is observed after 4 hours of Raman measurements. While the degradation of the sample does not seem to strongly impact the main features of the Raman spectrum, we optimized the laser power and integration time to extract the best possible Raman spectra resulting in lower sample degradation.

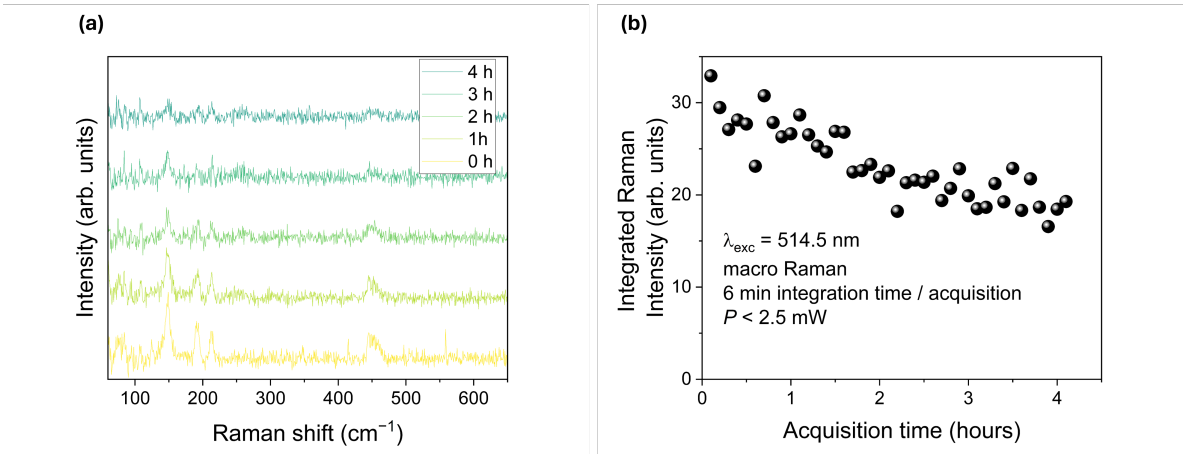


**Fig. S11:** (a) Raman spectra at ambient conditions measured with different acquisition times. (b) Total integrated intensity after subtraction of a smooth background.

## 4.4 Calculated phonon modes

**Table S2:** Calculated phonon wavenumbers at 0 GPa. Infrared active modes ($A_u$ and $B_u$) have also been included

| $A_g$ (cm$^{-1}$) | $B_g$ (cm$^{-1}$) | $A_u$ (cm$^{-1}$) | $B_u$ (cm$^{-1}$) |
|---|---|---|---|
| 25.438 | 25.226 | 16.044 | 13.945 |
| 38.371 | 41.256 | 35.682 | 50.016 |
| 48.47 | 48.918 | 57.822 | 58.68 |
| 70.05 | 69.902 | 62.429 | 81.28 |
| 76.906 | 79.828 | 83.574 | 89.657 |
| 106.266 | 100.491 | 89.358 | 97.275 |
| 120.789 | 117.671 | 98.039 | 127.247 |
| 130.579 | 132.706 | 124.514 | 141.742 |
| 138.294 | 137.882 | 143.231 | 156.594 |
| 157.062 | 154.86 | 161.411 | 173.864 |
| 176.603 | 175.502 | 175.671 | 284.601 |
| 198.031 | 196.799 | 285.1 | 404.449 |
| 412.086 | 411.802 | 405.967 | 429.132 |
| 420.119 | 418.371 | 431.926 | - |
| 439.21 | 437.741 | - | - |

# References


[1] L. Liao, E. Kovalska, V. Mazanek, L. Valdman, L. Dekanovský, W. Bing, D. Sedmidubský, J. Luxa, Štěpán Huber, A. P. Herman, R. Kudrawiec and Z. Sofer, *J. Mater. Chem. C*, 2022, **10**, 8834–8844.

[2] N. Sorogas, K. Tersis, A. Michail, S. Ves, K. Papagelis, D. Christofilos and J. Arvanitidis, *Crystals*, 2025, **15**, 1056.

[3] J. S. W. Holtz, R. W. Bormett, Z. Chi, N. Cho, X. G. Chen, V. Pajcini, S. A. Asher, L. Spinelli, P. Owen and M. Arrigoni, *Appl. Spectrosc.*, 1996, **50**, 1459–1468.

[4] M. Z. Jandali, G. Eulenberger and H. Hahn, *Z. Anorg. Allg. Chem.*, 1978, **447**, 105–118.

[5] D. Louër and A. Boultif, *Powder Diffr.*, 2014, **29**, S7–S12.

[6] J. Rodriguez-Carvajal, J. Gonzalez-Platas and N. A. Katcho, *Acta Crystallogr., Sect. B*, 2025, **81**, 302–317.

[7] M. U. Cohen, *Rev. Sci. Instrum.*, 1935, **6**, 68–74.

[8] M. Cardona, *Light Scattering in Solids I*, Springer, Berlin, 1983.

[9] Y.-L. Chuang, Y.-T. Yao, B.-C. Yang, C.-S. Lue, C.-N. Kuo, M.-L. Lee and J.-K. Sheu, *Chinese J. Phys.*, 2025, **93**, 409–417.